

Contrastive Similarity Matching for Supervised Learning

Shanshan Qin¹, Nayantara Mudur², and Cengiz Pehlevan¹

¹John A. Paulson School of Engineering and Applied Sciences,
Harvard University, Cambridge, MA USA

²Department of Physics, Harvard University, Cambridge, MA USA

Abstract

We propose a novel biologically-plausible solution to the credit assignment problem motivated by observations in the ventral visual pathway and trained deep neural networks. In both, representations of objects in the same category become progressively more similar, while objects belonging to different categories become less similar. We use this observation to motivate a layer-specific learning goal in a deep network: each layer aims to learn a representational similarity matrix that interpolates between previous and later layers. We formulate this idea using a contrastive similarity matching objective function and derive from it deep neural networks with feedforward, lateral, and feedback connections, and neurons that exhibit biologically-plausible Hebbian and anti-Hebbian plasticity. Contrastive similarity matching can be interpreted as an energy-based learning algorithm, but with significant differences from others in how a contrastive function is constructed.

1 Introduction

Synaptic plasticity is generally accepted as the underlying mechanism of learning in the brain, which almost always involves a large population of neurons and synapses across many different brain regions. How the brain modifies and coordinates individual synapses in the face of limited information available to each synapse in order to achieve a global learning task, the credit assignment problem, has puzzled scientists for decades. A major effort in this domain has been to look for a biologically-plausible implementation of the back-propagation of error algorithm (BP) (Rumelhart et al., 1986), which has long been disputed due to its

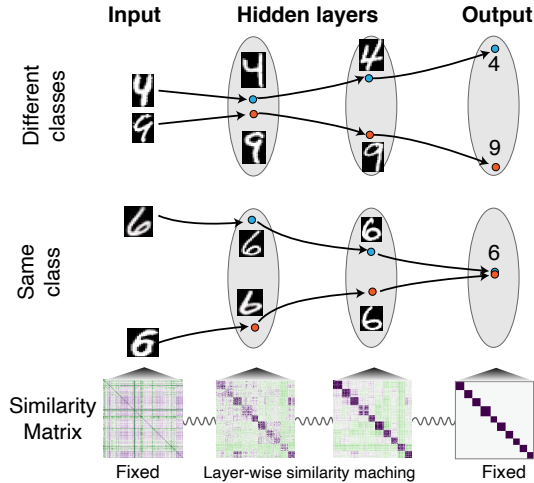


Figure 1: Supervised learning via layer-wise similarity matching. For inputs of different categories, similarity-matching differentiates the representations progressively (top), while for objects of the same category, representations become more and more similar (middle). For a given set of training data and their corresponding labels, the training process can be regarded as learning hidden representations whose similarity matrices match that of both input and output (bottom). The tuning of representational similarity is indicated by the springs with the constraints that input and output similarity matrices are fixed.

biological implausibility (Crick, 1989), although recent studies have made progress in resolving some of these concerns (Xie and Seung, 2003; Lee et al., 2015; Lillicrap et al., 2016; Nøkland, 2016; Scellier and Bengio, 2017; Guerguiev et al., 2017; Whittington and Bogacz, 2017; Sacramento et al., 2018; Richards and Lillicrap, 2019; Whittington and Bogacz, 2019; Belilovsky et al., 2018; Ororbia and Mali, 2019; Lillicrap et al., 2020).

In this paper, we present a novel approach to the credit assignment problem, motivated by observations on the nature of hidden layer representations in the ventral visual pathway of the brain and deep neural networks. In both, representations of objects belonging to different categories become less similar, while representations of objects belonging to the same category become more similar (Grill-Spector and Weiner, 2014; Kriegeskorte et al., 2008; Yamins and DiCarlo, 2016). In other words, categorical clustering of representations becomes more and more explicit in the later layers (Fig. 1). These results suggest a new approach to the credit assignment problem. By assigning each layer a layer-local similarity matching task (Pehlevan and Chklovskii, 2019; Obeid et al., 2019), whose goal is to learn an intermediate representational similarity matrix between previous and later layers, we may be able to get away from the need of backward propagation

of errors (Fig. 1). Motivated by this idea and previous observations that error signal can be implicitly propagated via the change of neural activities (Hinton and McClelland, 1988; Scellier and Bengio, 2017), we propose a biologically plausible supervised learning algorithm, the contrastive similarity matching (CSM) algorithm.

Contrastive training (Anderson and Peterson, 1987; Movellan, 1991; Baldi and Pineda, 1991) has been used to learn the energy landscapes of neural networks (NNs) whose dynamics minimize an energy function. Examples include influential algorithms like the Contrastive Hebbian Learning (CHL) (Movellan, 1991) and Equilibrium Propagation (EP) (Scellier and Bengio, 2017), where weight-updates rely on the difference of the neural activity between a free phase, and a clamped (CHL) or nudged (EP) phase to locally approximate the gradient of an error signal. The learning process can be interpreted as minimizing a contrastive function, which reshapes the energy landscape to eliminate spurious fixed points and makes the desired fixed point more stable.

The CSM algorithm applies this idea to a contrastive function formulated by nudging the output neurons of a multilayer similarity matching objective function (Obeid et al., 2019). As a consequence, the hidden layers learn intermediate representations between their previous and later layers. From the CSM contrastive function, we derive deep neural networks with feedforward, lateral and feedback connections, and neurons that exhibit biologically-plausible Hebbian and anti-Hebbian plasticity.

The nudged phase of the CSM algorithm is analogous to the nudged phase of EP but different. It performs Hebbian feedforward and anti-Hebbian lateral updates. CSM has opposite sign for the lateral connection updates compared with EP and CHL. This is because our weight updates solve a minimax problem. Anti-Hebbian learning pushes neurons within a layer to learn different representations. The free phase of CSM is also different where only feedforward weights are updated by an anti-Hebbian rule. In EP and CHL all weights are updated.

Our main contributions and results are listed below:

- We provide a novel approach to the credit assignment problem using biologically-plausible learning rules by generalizing the similarity matching principle (Pehlevan and Chklovskii, 2019) to supervised learning tasks and introducing the Contrastive Similarity Matching algorithm.
- The proposed supervised learning algorithm can be related to other energy-based algorithms, but with a distinct underlying mechanism.
- We present a version of our neural network algorithm with structured connectivity.

- We show that the performance of our algorithm is on par with other energy-based algorithms using numerical simulations. The learned representations of our Hebbian/anti-Hebbian network is sparser.

The rest of this paper is organized as follows. In Section 2, to illustrate our main ideas we introduce and discuss supervised similarity matching. We then introduce nudged deep similarity matching objective, from which we derive the CSM algorithm for deep neural networks with nonlinear activation functions and structured connectivity. We discuss the relation of CSM to other energy-based learning algorithms. In Section 3, we report the performance of CSM and compare it with EP, highlighting the differences between them. Finally, we discuss our results, possible biological mechanisms, and relate them to other works in Section 4.

2 Contrastive Similarity Matching for Deep Non-linear Networks

2.1 Warm Up: Supervised Similarity Matching Objective

Here we illustrate our main idea in a simple setting. Let $\mathbf{x}_t \in \mathbb{R}^n$, $t = 1, \dots, T$ be a set of data points and $\mathbf{z}_t^l \in \mathbb{R}^k$ be their corresponding desired output or labels. Our idea is that the representation learned by the hidden layer, $\mathbf{y}_t \in \mathbb{R}^m$, should be half-way between the input \mathbf{x} and the desired output \mathbf{z}^l . We formulate this idea using representational similarities, quantified by the dot product of representational vectors within a layer. Our proposal can be formulated as the following optimization problem, which we name supervised similarity matching:

$$\min_{\{\mathbf{y}_t\}_{t=1}^T} \frac{1}{T^2} \sum_{t=1}^T \sum_{t'=1}^T [(\mathbf{x}_t^\top \mathbf{x}_{t'} - \mathbf{y}_t^\top \mathbf{y}_{t'})^2 + (\mathbf{y}_t^\top \mathbf{y}_{t'} - \mathbf{z}_t^{l\top} \mathbf{z}_{t'}^l)^2]. \quad (1)$$

To get an intuition about what this cost function achieves, consider the case where only one training datum exists. Then, $\mathbf{y}_1^\top \mathbf{y}_1 = \frac{1}{2}(\mathbf{x}_1^\top \mathbf{x}_1 + \mathbf{z}_1^{l\top} \mathbf{z}_1^l)$, satisfying our condition. When multiple training data are involved, interactions between different data points lead to a non-trivial solution, but the fact that the hidden layer representations are in between the input and output layers stays.

The optimization problem (1) can be analytically solved, making our intuition precise. Let the representational similarity matrix of the input layer be $R_{tt'}^x \equiv \mathbf{x}_t^\top \mathbf{x}_{t'}$, the hidden layer be $R_{tt'}^y \equiv \mathbf{y}_t^\top \mathbf{y}_{t'}$, and the output layer be $R_{tt'}^z \equiv \mathbf{z}_t^{l\top} \mathbf{z}_{t'}^l$. Instead of solving \mathbf{y} directly, we can reformulate and solve the supervised similarity matching problem (1) for \mathbf{R}^y , and then obtain \mathbf{y} s by a matrix factorization through

an eigenvalue decomposition. By completing the square, problem (1) becomes an optimization problem for \mathbf{R}^y :

$$\min_{\mathbf{R}^y \in \mathcal{S}^m} \frac{1}{T^2} \left\| \frac{1}{2} (\mathbf{R}^x + \mathbf{R}^z) - \mathbf{R}^y \right\|_F^2, \quad (2)$$

where \mathcal{S}^m is the set of symmetric matrices with rank m , and F denotes the Frobenius norm. Optimal \mathbf{R}^y is given by keeping the top m modes in the eigenvalue decomposition of $\frac{1}{2} (\mathbf{R}^x + \mathbf{R}^z)$ and setting the rest to zero. If $m \geq \text{rank}(\mathbf{R}^x + \mathbf{R}^z)$, then optimal \mathbf{R}^y exactly equals $\frac{1}{2} (\mathbf{R}^x + \mathbf{R}^z)$, achieving a representational similarity matrix that is the average of input and output layers.

The supervised similarity matching problem (1) can be solved by an online algorithm that can in turn be mapped onto the operation of a biologically plausible network with a single hidden layer, which runs an attractor dynamics minimizing an energy function (see Appendix A for details). This approach can be generalized to multi-layer and nonlinear networks. We do not pursue it further because the resulting algorithm does not perform as well due to spurious fixed points of nonlinear dynamics for a given input \mathbf{x}_t . The Contrastive Similarity Matching algorithm overcomes this problem.

2.2 Nudged Deep Similarity Matching Objective and Its Dual Formulation

Our goal is to combine the ideas of supervised similarity matching and contrastive learning to derive a biologically plausible supervised learning algorithm. To do so, we define the nudged similarity matching problem first.

In energy-based learning algorithms like CHL and EP, weight-updates rely on the difference of neural activity between a free phase and a clamped/nudged phase to locally approximate the gradient of an error signal. This process can be interpreted as minimizing a contrastive function, which reshapes the energy landscape to eliminate the spurious fixed points and make the fixed point corresponding to the desired output more stable. We adopt this idea to introduce what we call the nudged similarity matching cost function, and derive its dual formulation, which will be the energy function used in our contrastive formulation.

We consider a P -layer ($P - 1$ hidden layers) NN with nonlinear activation functions, f . For notational convenience, we denote inputs to the network by $\mathbf{r}^{(0)}$, outputs by $\mathbf{r}^{(P)}$, and activities of hidden layers by $\mathbf{r}^{(p)}$, $p = 1, \dots, P - 1$. We propose the following objective function for the training phase where outputs are

nudged toward the desired labels \mathbf{z}_t^l

$$\begin{aligned} & \min_{\substack{a_1 \leq \mathbf{r}_t^p \leq a_2 \\ t=1, \dots, T \\ p=1, \dots, P}} \sum_{p=1}^P \frac{\gamma^{p-P}}{2T^2} \sum_{t=1}^T \sum_{t'=1}^T \|\mathbf{r}_t^{(p-1)\top} \mathbf{r}_{t'}^{(p-1)} - \mathbf{r}_t^{(p)\top} \mathbf{r}_{t'}^{(p)}\|_2^2 + \sum_{p=1}^P \frac{2\gamma^{p-P}}{T} \sum_{t=1}^T \mathbf{F}(\mathbf{r}_t^{(p)})^\top \mathbf{1} \\ & + \frac{2\beta}{T} \sum_{t=1}^T \|\mathbf{r}_t^{(P)} - \mathbf{z}_t^l\|_2^2. \end{aligned} \quad (3)$$

Here, β is a control parameter that specifies how strong the nudge is. $\beta \rightarrow \infty$ limit corresponds to clamping the output layer to the desired output. $\gamma \geq 0$ is a parameter that controls the influence of the later layers to the previous layers. $F(\mathbf{r}_t^{(p)})$ is a regularizer defined and related to the activation function by $dF(\mathbf{r}_t^{(p)})/d\mathbf{r}_t^{(p)} = \mathbf{u}_t^{(p)} - \mathbf{b}_t^{(p)}$, where $\mathbf{r}_t^{(p)} = f(\mathbf{u}_t^{(p)})$, $\mathbf{u}_t^{(p)}$ and $\mathbf{r}_t^{(p)}$ are the total input and output of p -th layer respectively, $\mathbf{b}_t^{(p)}$ is the threshold of neurons in layer p . The reason for the inclusion of this regularizer will be apparent below. We assume f to be a monotonic and bounded function, whose bounds are given by a_1 and a_2 .

The objective function (3) is almost identical to the deep similarity matching objective introduced in (Obeid et al., 2019), except the nudging term. Obeid et al. (2019) used $\beta = 0$ version as an unsupervised algorithm. Here, we use a non-zero β for supervised learning.

We note that we have not made a reference to a particular neural network yet. This is because the neural network that optimizes (3) will be fully derived from the nudged similarity matching problem. It will not be prescribed as in traditional approaches to deep learning. We next describe how to do this derivation.

Using the duality transforms introduced in (Pehlevan et al., 2018; Obeid et al., 2019), the above nudged supervised deep similarity matching problem (3) can be turned into a dual minimax problem:

$$\min_{\{\mathbf{W}^{(p)}\}} \max_{\{\mathbf{L}^{(p)}\}} \frac{1}{T} \sum_{t=1}^T l_t \left(\{\mathbf{W}^{(p)}\}, \{\mathbf{L}^{(p)}\}, \mathbf{r}_t^{(0)}, \mathbf{z}_t^l, \beta \right), \quad (4)$$

where

$$\begin{aligned} l_t := & \min_{\substack{a_1 \leq \mathbf{r}_t^{(p)} \leq a_2 \\ p=1, \dots, P}} \sum_{p=1}^P \gamma^{p-P} \left[\text{Tr} \mathbf{W}^{(p)\top} \mathbf{W}^{(p)} - 2\mathbf{r}_t^{(p)\top} \mathbf{W}^{(p)} \mathbf{r}_t^{(p-1)} \right. \\ & \left. + \frac{1 + \gamma(1 - \delta_{pP})}{2} c^{(p)} \left(2\mathbf{r}_t^{(p)\top} \mathbf{L}^{(p)} \mathbf{r}_t^{(p)} - \text{Tr} \mathbf{L}^{(p)\top} \mathbf{L}^{(p)} \right) + 2\mathbf{F} \left(\mathbf{r}_t^{(p)} \right)^\top \mathbf{1} \right] + 2\beta \|\mathbf{r}_t^{(P)} - \mathbf{z}_t^l\|_2^2, \end{aligned} \quad (5)$$

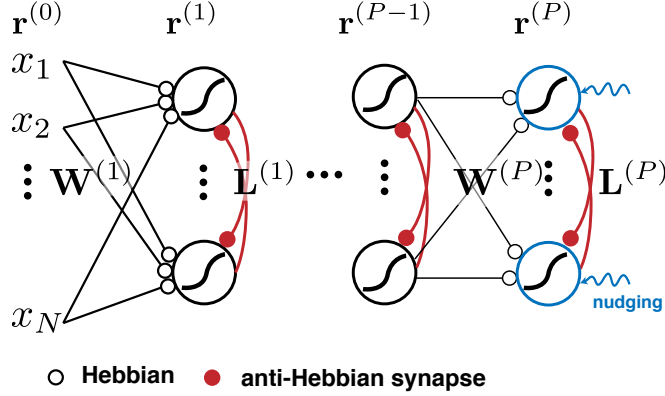


Figure 2: Illustration of the Hebbian/anti-Hebbian network with P hidden layers that implements the contrastive similarity matching algorithm. The output layer neurons alternate between the free phase and nudged phase.

Here, we introduced $c^{(p)}$ as a parameter that governs the relative importance of forward versus recurrent inputs and $c^{(p)} = 1$ corresponds to the exact transformation, details of which is given in the Appendix B.

In Appendix C, we show that the the objective of the min in l_t defines an energy function for a deep neural network with feedforward, lateral and feedback connections (Figure 2). It has following neural dynamics:

$$\begin{aligned} \tau_p \frac{d\mathbf{u}^{(p)}}{dt} &= -\mathbf{u}^{(p)} + \mathbf{W}^{(p)} \mathbf{r}_t^{(p-1)} - c^{(p)} [1 + \gamma(1 - \delta_{pP})] \mathbf{L}^{(p)} \mathbf{r}_t^{(p)} + \mathbf{b}_t^{(p)} \\ &\quad + \gamma(1 - \delta_{pP}) \mathbf{W}^{(p+1)\top} \mathbf{r}_t^{(p+1)} - 2\beta \delta_{pP} (\mathbf{r}_t^{(P)} - \mathbf{z}_t^l), \\ \mathbf{r}_t^{(p)} &= \mathbf{f}(\mathbf{u}^{(p)}), \end{aligned} \quad (6)$$

where δ_{pP} is the Kronecker delta, $p = 1, \dots, P$, τ_p is a time constant, $\mathbf{W}^{(P+1)} = \mathbf{0}$, $\mathbf{r}_t^{(P+1)} = \mathbf{0}$. Therefore, the minimization can be performed by running the dynamics until convergence. This observation will be the building block of our CSM algorithm, which we present below. Finally, we note that the introduction of the regularizer in (3) is necessary for the energy interpretation and for proving the convergence of the neural dynamics (Obeid et al., 2019).

2.3 Contrastive Similarity Matching

We first state our contrastive function and then discuss its implications. We suppress the dependence on training data in l_t and define:

$$\{\mathbf{L}^{*(p)}\} \equiv \arg \max_{\{\mathbf{L}^{(p)}\}} \frac{1}{T} \sum_{t=1}^T l_t(\{\mathbf{W}^{(p)}\}, \{\mathbf{L}^{(p)}\}, \{\mathbf{b}^{(p)}\}, \beta), \quad (7)$$

and

$$E(\{\mathbf{W}^{(p)}\}, \{\mathbf{b}^{(p)}\}, \beta) = \frac{1}{T} \sum_{t=1}^T l_t(\{\mathbf{W}^{(p)}\}, \{\mathbf{L}^{*(p)}\}, \{\mathbf{b}^{(p)}\}, \beta). \quad (8)$$

Finally, we formulate our contrastive function as

$$J^\beta(\{\mathbf{W}^{(p)}\}, \{\mathbf{b}^{(p)}\}) = E(\beta) - E(0), \quad (9)$$

which is to be minimized over feedforward and feedback weights $\{\mathbf{W}^{(p)}\}$, as well as bias $\{\mathbf{b}^{(p)}\}$. For fixed bias, minimization of the first term, $E(\beta)$ corresponds exactly to the optimization of the minimax dual of nudged deep similarity matching (4). The second term $E(0)$ corresponds to a free phase, where no nudging is applied. We note that in order to arrive at a contrastive minimization problem, we use the same optimal lateral weights, (7), from the nudged phase in the free phase. Compared to the minimax dual of nudged deep similarity matching (4), we also optimize it over the bias for better performance.

Minimization of the contrastive function (9) closes the energy gap between nudged and free phases. Because the energy functions are evaluated at the fixed point of the neural dynamics (6), such procedure enforces the output of the nudged network to be a fixed point of the free neural dynamics.

To optimize our contrastive function (9) in a stochastic (one training datum at a time) manner, we use the following procedure. For each pair of training data $\{\mathbf{r}_t^0, \mathbf{z}_t^l\}$, we run the nudged phase ($\beta \neq 0$) dynamics (6) until convergence to get the fixed point $\mathbf{r}_{\beta,t}^{(p)}$. Next, we run the free phase ($\beta = 0$) neural dynamics (6) until convergence. We collect the fixed points $\mathbf{r}_{0,t}^{(p)}$. $\mathbf{L}^{(p)}$ is updated following a gradient ascent of (7), while $\mathbf{W}^{(p)}$ and $\mathbf{b}^{(p)}$ follow a gradient descent of (9):

$$\begin{aligned} \Delta \mathbf{L}^{(p)} &\propto \left(\mathbf{r}_{\beta,t}^{(p)} \mathbf{r}_{\beta,t}^{(p)\top} - \mathbf{L}^{(p)} \right), \\ \Delta \mathbf{W}^{(p)} &\propto \left(\mathbf{r}_{\beta,t}^{(p)} \mathbf{r}_{\beta,t}^{(p-1)\top} - \mathbf{r}_{0,t}^{(p)} \mathbf{r}_{0,t}^{(p-1)\top} \right), \\ \Delta \mathbf{b}^{(p)} &\propto \left(\mathbf{r}_{\beta,t}^{(p)} - \mathbf{r}_{0,t}^{(p)} \right). \end{aligned} \quad (10)$$

In practice, learning rates can be chosen differently to achieve the best performance. A constant prefactor before $\mathbf{L}^{(p)}$ can be added to achieve numerical stability. The above CSM algorithm is summarized in Algorithm 1.

2.3.1 Relation to Gradient Descent

The CSM algorithm can be related to gradient descent in the $\beta \rightarrow 0$ limit using similar arguments as in (Scellier and Bengio, 2017). To see this explicitly, we first simplify the notation by collecting all $\mathbf{W}^{(p)}$ and $\mathbf{b}^{(p)}$ parameters under one vector

Algorithm 1 Constrative Similarity Matching (CSM)

Input: Initial $\{\mathbf{W}^{(p)}\}$, $\{\mathbf{L}^{(p)}\}$, $\{\mathbf{b}^{(p)}\}$, $\{\mathbf{r}^{(p)}\}$, $p = 1, \dots, P$

for $t = 1$ **to** T **do**

Run the nudged phase neural dynamics (6) with $\beta \neq 0$ until convergence, collect the fixed point $\{\mathbf{r}_{\beta,t}^{(p)}\}$

Run the free phase dynamics (6) with $\beta = 0$ until convergence, collect fixed point $\{\mathbf{r}_{0,t}^{(p)}\}$

Update $\{\mathbf{L}^{(p)}\}$, $\{\mathbf{W}^{(p)}\}$ and $\{\mathbf{b}^{(p)}\}$ according to (10).

end for

variable $\boldsymbol{\theta}$, denote all the lateral connection matrices defined in (7) by \mathbf{L}^* , and represent the fixed points of the network by $\bar{\mathbf{r}}$. Now the energy function can be written as $E(\boldsymbol{\theta}, \beta; \mathbf{L}^*, \bar{\mathbf{r}})$, where \mathbf{L}^* and $\bar{\mathbf{r}}$ depend on $\boldsymbol{\theta}$ and β implicitly. In the limit of small β , one can approximate the energy function to leading order by

$$E(\boldsymbol{\theta}, \beta; \mathbf{L}^*, \bar{\mathbf{r}}) \approx E(\boldsymbol{\theta}, 0) + \left(\text{Tr} \left(\frac{\partial E}{\partial \mathbf{L}^*} \frac{\partial \mathbf{L}^*}{\partial \beta} \right) + \frac{\partial E}{\partial \bar{\mathbf{r}}} \cdot \frac{\partial \bar{\mathbf{r}}}{\partial \beta} + \frac{\partial E}{\partial \beta} \right) \Big|_{\beta=0} \beta. \quad (11)$$

Note that the maximization in (7) implies $\frac{\partial E}{\partial \mathbf{L}^*} = \mathbf{0}$. If $\frac{\partial E}{\partial \bar{\mathbf{r}}}$ is also $\mathbf{0}$, i.e. the minima of (5) are not on the boundaries but at the interior of the feasible set, then in the limit $\beta \rightarrow 0$, the gradient of the contrastive function is the gradient of the mean square error function with respect to $\boldsymbol{\theta}$:

$$\lim_{\beta \rightarrow 0} \frac{1}{\beta} \frac{\partial J}{\partial \boldsymbol{\theta}} = \frac{\partial}{\partial \boldsymbol{\theta}} \frac{\partial E}{\partial \beta} \Big|_{\beta=0} = \frac{\partial}{\partial \boldsymbol{\theta}} \frac{1}{T} \sum_{t=1}^T \|\bar{\mathbf{r}}_t^P - \mathbf{z}_t^l\|_2^2. \quad (12)$$

It is important to note that while $\beta \rightarrow 0$ limit of CSM is related to gradient descent, this limit is not necessarily the best performing one (as also observed in (Scellier and Bengio, 2017) for EP) and β is a hyperparameter to be tuned. In Appendix F, we present simulations that confirm the existence of an optimal β away from $\beta = 0$.

2.3.2 Relation to Other Energy Based Learning Algorithms

The CSM algorithm is similar in spirit to other contrastive algorithms, such as CHL and EP. Like these algorithms, CSM performs two runs of the neural dynamics in a “free” and a “nudged” phase. However, there are important differences. One major difference is that in CSM, the contrastive function is minimized by the feedforward weights. The lateral weights take part in the maximization of a different minimax objective (7). In CHL and EP, such minimization is done with respect to all the weights.

As a consequence of this difference, CSM uses a different update for lateral weights than CHL and EP. This anti-Hebbian update is different in two ways: 1) It has the opposite sign, i.e. EP and CHL nudged/clamped phase lateral updates are Hebbian. 2) No update is applied in the free phase. As we will demonstrate in numerical simulations, our lateral update imposes a competition between different units in the same layer. When network activity is constrained to be nonnegative, such lateral interactions are inhibitory and sparsify neural activity.

Analogous of two hyperparameters of our algorithm play special roles in EP and CHL. The $\beta \rightarrow \infty$ limit of EP corresponds to clamping the output to the desired value in the nudged phase (Scellier and Bengio, 2017). Similarly, the $\beta \rightarrow \infty$ limit of CSM also corresponds to training with fully clamped output units. We discussed the gradient descent interpretation of the $\beta \rightarrow 0$ limits of both algorithms above. CHL is equivalent to backpropagation when feedback strength, the analog of our γ parameter, vanishes (Xie and Seung, 2003). In CSM, γ is a hyperparameter to be tuned, which we explore in Appendix F.

2.4 Introducing structured connectivity

We can also generalize the nudged supervised similarity matching (Eq.3) to derive a Hebbian/anti-Hebbian network with structured connectivity. Following Obeid et al. (2019), we can modify any of the cross terms in the layer-wise similarity matching objective (Eq.3) by introducing synapse-specific structure constants. For example:

$$-\frac{1}{T^2} \sum_i^{N^{(p)}} \sum_j^{N^{(p-1)}} \sum_t^T \sum_{t'}^T r_{t,i}^{(p)} r_{t',i}^{(p)} r_{t,j}^{(p-1)} r_{t',j}^{(p-1)} s_{ij}^W, \quad (13)$$

where $N^{(p)}$ is the number of neurons in p -th layer, $s_{ij}^W \geq 0$ are constants that set the structure of feedforward weight matrix between p -th layer and $(p-1)$ -th layer. In particular, setting them to zero removes the connection, without changing the interpretation of energy function (Obeid et al., 2019). Similarly, we can introduce constants s_{ij}^L to specify the structure of the lateral connections (Fig. 6 A). Using such structure constants, one can introduce many different architectures, some of which we experiment with below. We present a detailed explanation of these points in Appendix C.

3 Numerical Simulations

In this section, we report the simulation results of the CSM algorithm on a supervised classification task using the MNIST dataset of handwritten digits (LeCun et al., 2010) and the CIFAR-10 image dataset (Krizhevsky et al., 2009). For our

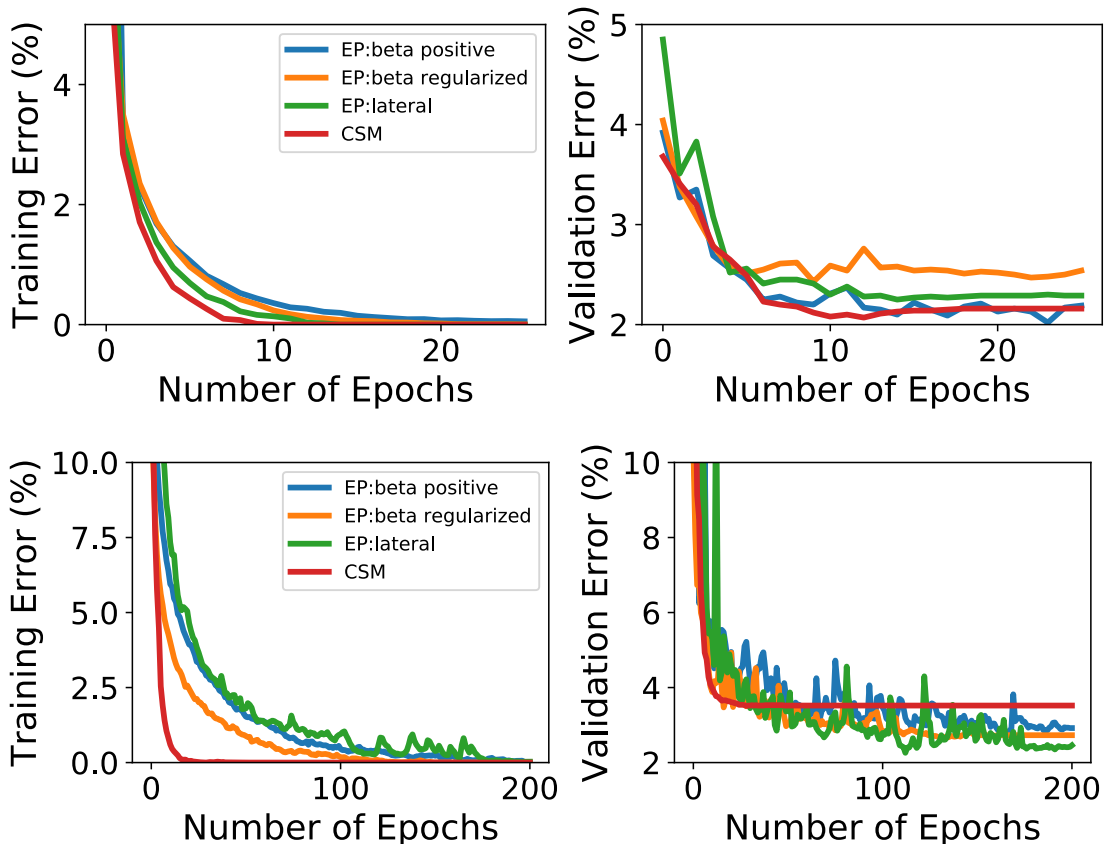


Figure 3: Comparison of training (left) and validation (right) errors between CSM and EP algorithms for a network with one hidden layer (784-500-10, upper panels) and three hidden layers (784-500-500-500-10, lower panels) trained on the MNIST dataset.

simulations, we used the Theano Deep Learning framework (Team et al., 2016) and modified the code released by Scellier and Bengio (2017). The activation functions of the units were $f(x) = \min\{1, \max\{x, 0\}\}$ and $c^{(p)} = 1/2(1 - \delta_{pP})$. Following Scellier and Bengio (2017), we used the persistent particle technique to tackle the long period of free phase relaxation. We stored the fixed points of hidden layers at the end of the free phase and used them to initialize the state of the network in the next epoch.

3.1 MNIST

The inputs consist of gray-scale 28-by-28 pixel images, and each image is associated with a label ranging from $\{0, \dots, 9\}$. We encoded the labels \mathbf{z}^l as one-hot 10-dimensional vectors. We trained fully connected NNs with one and three hid-

den layers with lateral connections within each hidden layer. The performance of CSM algorithm was compared with several variants of EP algorithm: (1) EP: beta regularized, where the networks had no lateral connections and the sign of β was randomized to act as a regularizer as in (Scellier and Bengio, 2017) ; (2) EP: beta positive, where the networks had no lateral connections and β was a positive constant; (3) EP: lateral, where networks had lateral connections and were trained with a positive constant β . In all the fully-connected network simulations for MNIST, the number of neurons in each hidden layer is 500. We attained 0% training error and 2.16% and 3.52% validation errors with CSM, in the one and three hidden layer cases respectively. This is on par with the performance of the EP algorithm, which attains a validation error of 2.53% and 2.73% respectively for variant 1 and 2.18% and 2.77% for variant 2 (Fig.3). In the 3-layer case, a training error-dependent adaptive learning rate scheme (CSM-Adaptive) was used, wherein the learning rate for the lateral updates is successively decreased when the training error drops below certain thresholds (see Appendix D for details).

3.2 CIFAR-10

CIFAR-10 is a more challenging dataset that contains 32-by-32 RGB images of objects belonging to ten classes of animals and vehicles. For fully connected networks, the performance of CSM was compared with EP (positive constant β). We obtain validation errors of 59.21% and 51.76% in the one and two hidden layer networks respectively in CSM, and validation errors of 57.60% and 53.43% in EP (Fig.4). The mean and standard errors on the mean, of the last twenty validation errors, are reported here, in order to account for fluctuations about the mean. It is interesting to note that for both algorithms, deeper networks perform better for CIFAR-10, but not for MNIST. For both datasets, the best performing network trained with CSM achieves slightly better validation accuracy than the best performing network trained with EP. The errors corresponding to the fully connected networks for both algorithms and datasets are summarized in Table 1. Here, CSM has been compared to the variant of EP with $\beta > 0$.

For CIFAR-10, the CSM algorithm with two hidden layers has a validation error around 51% after 1000 epochs but was run for a total of 3584 epochs since the training error was still decreasing. The simulation does not reach zero training error, but starts plateauing at around 18%, with a decrease of only 0.3% for the last 100 epochs. The validation error does not decrease with the additional training beyond 1000 epochs. It is possible that better validation accuracy could be reached if better training errors were achieved e.g. by better performing learning rate schedules.

Table 1: Comparison of the training and validation errors of fully connected networks for EP (beta positive) and CSM. For both algorithms, the best performing networks correspond to two hidden layer networks for CIFAR-10 and one hidden layer networks for MNIST. Here, xHL means that the network has x hidden layers. For the CIFAR-10, CSM, 2HL simulation, errors at the end of 3584 epochs are reported. For the other CIFAR-10 simulations, errors at the end of 1000 epochs are reported.

MNIST			CIFAR-10		
RULE	TRAIN (%)	VALIDATE (%)	RULE	TRAIN (%)	VALIDATE (%)
CSM:1HL	0.00	2.16	CSM:1HL	1.77	59.21 \pm 0.08
EP:1HL	0.03	2.18	EP:1HL	0.76	57.60 \pm 0.06
CSM:3HL	0.00	3.52	CSM:2HL	17.96	51.76 \pm 0.002
EP:3HL	0.00	2.77	EP:2HL	1.25	53.43 \pm 0.04

3.3 Neuronal Representations

While CSM and EP perform similarly, their learned representations differ in sparseness (Fig.5). Due to the non-negativity of hidden unit activity and anti-Hebbian lateral updates, the CSM network ends up with inhibitory lateral connections, which enforce sparse response (Fig.5). This can also be seen from the similarity matching objective (3). Imagine there are only two inputs with a negative dot product, $\mathbf{x} \cdot \mathbf{x}' < 0$. The next layer will at least partially match this dot product, however, because the lowest value of $\mathbf{y} \cdot \mathbf{y}'$ is zero due to $\mathbf{y}, \mathbf{y}' \geq 0$, \mathbf{y} and \mathbf{y}' will be forced to be orthogonal with non-overlapping sets of active neurons. Sparse response is a general feature of cortical neurons (Olshausen and Field, 2004) and energy-efficient, making the representations learned by CSM more biologically relevant.

3.4 Structured Networks

We also examined the performance of CSM in networks with structured connectivity. Every hidden layer can be constructed by first considering sites arranged on a two-dimensional grid. Each site only receives inputs from selected nearby sites controlled by the radius parameter (Fig.6A). This setting resembles retinotopy (Kandel et al., 2000) in the visual cortex. Multiple neurons can be present at a single site controlled by the neurons per site (NPS) parameter. We consider lateral connections only between neurons sharing the same (x, y) coordinate.

For MNIST dataset, networks with structured connectivity trained with the CSM rule achieved 2.22% validation error for a single hidden layer network with a

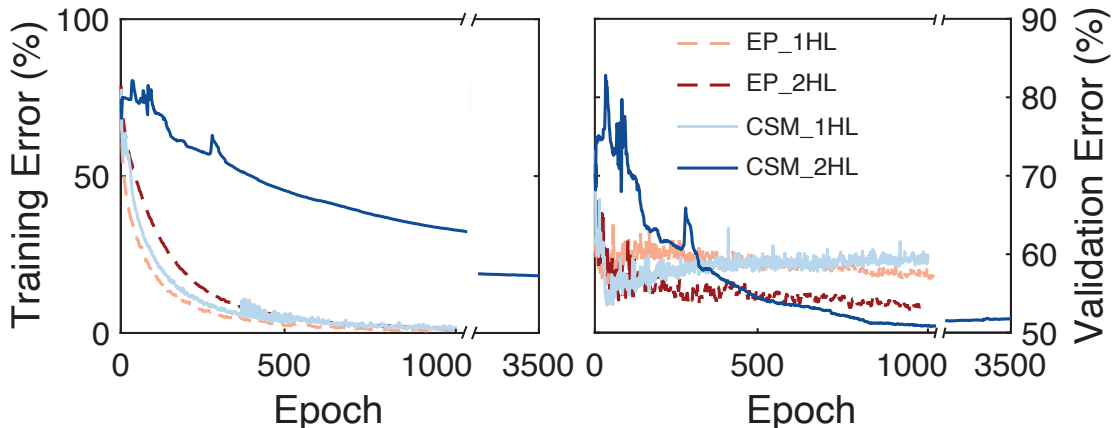


Figure 4: Training (left) and validation (right) error curves for fully connected networks trained on CIFAR-10 dataset with CSM (solid) and EP (dashed) algorithms. The best fully connected CSM network attains slightly better validation accuracy than the best fully connected EP network.

radius of 4 and NPS of 20 (Fig. 6B) (See Appendix D for details). For CIFAR-10 dataset, a one hidden layer structured network using CSM algorithm achieves 34% training error and 49.5% validation error after 250 epochs, which is a significant improvement compared to the fully connected one layer network. This structured network had a radius of 4 and NPS of 3. A two hidden layer structured network yielded a training error of 46.8% and a validation error of 51.4% after 200 epochs. Errors reported for the structured runs are the averages of five trials. The results for all fully connected and structured networks are reported in Appendix D and E.

4 Discussion

In this paper, we proposed a new solution to the credit assignment problem by generalizing the similarity matching principle to the supervised domain and proposed a biologically plausible supervised learning algorithm, the Contrastive Similarity Matching algorithm. In CSM, a supervision signal is introduced by minimizing the energy difference between a free phase and a nudged phase. CSM differs significantly from other energy-based algorithms in how the contrastive function is constructed. We showed that when non-negativity constraint is imposed on neural activity, the anti-Hebbian learning rule for the lateral connections makes the representations sparse and biologically relevant. We also derived the CSM algorithm for neural networks with structured connectivity.

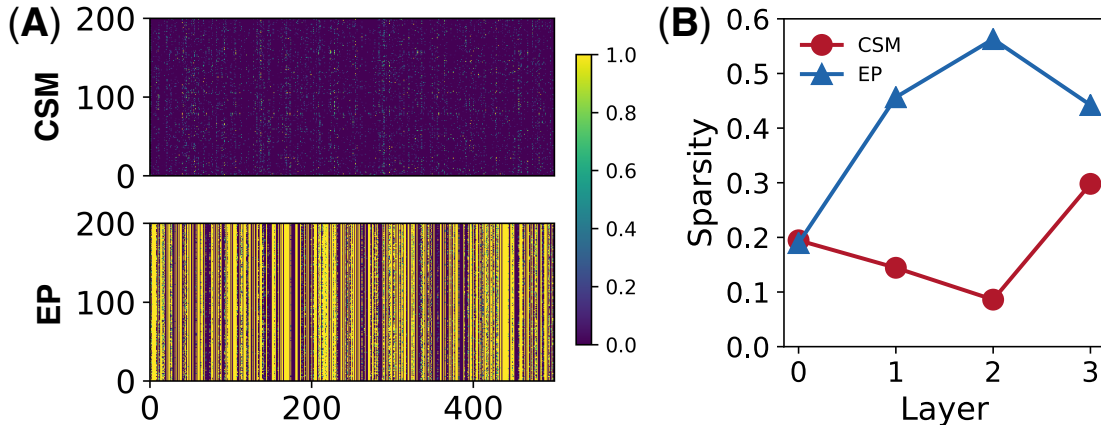


Figure 5: Representations of neurons in NNs trained by CSM algorithm are much sparser than that of EP algorithm on MNIST dataset. (A) Heatmaps of representations at the second hidden layer, each row is the response of 500 neurons to a given digit image. Upper: CSM algorithm. Lower: EP algorithm. (B) Representation sparsity, defined as fraction of neurons whose activity are larger than a threshold (0.01), along different layers. Layer 0 is the input. The network has a 784-500-500-500-10 architecture.

The idea of using representational similarity for training neural networks has taken various forms in previous work. The similarity matching principle has recently been used to derive various biologically plausible unsupervised learning algorithms (Pehlevan and Chklovskii, 2019), such as principal subspace projection (Pehlevan and Chklovskii, 2015), blind source separation (Pehlevan et al., 2017), feature learning (Obeid et al., 2019), and manifold learning (Sengupta et al., 2018). It has been used for semi-supervised classification (Genkin et al., 2019). Similarity matching has also been used as part of a local cost function to train a deep convolutional network (Nøkland and Eidnes, 2019), where instead of layer-wise similarity matching, each hidden layer aims to learn representations similar to the output layer. Representational similarity matrices derived from neurobiology data have recently been used to regularize CNNs trained for image classification. The resulting networks are more robust to noise and adversarial attacks (Li et al., 2019). It would be interesting to study the robustness of neural networks trained by the CSM algorithm.

Like other contrastive learning algorithms, CSM operates with two phases: free and nudged. Previous studies in contrastive learning provided various biologically possible implementations of such two phased learning. One proposal is to introduce the teacher signal into the network through an oscillatory coupling with a period longer than the time scale of neural activity converging to a steady state. Baldi and Pineda (1991) proposed that such oscillations might be related

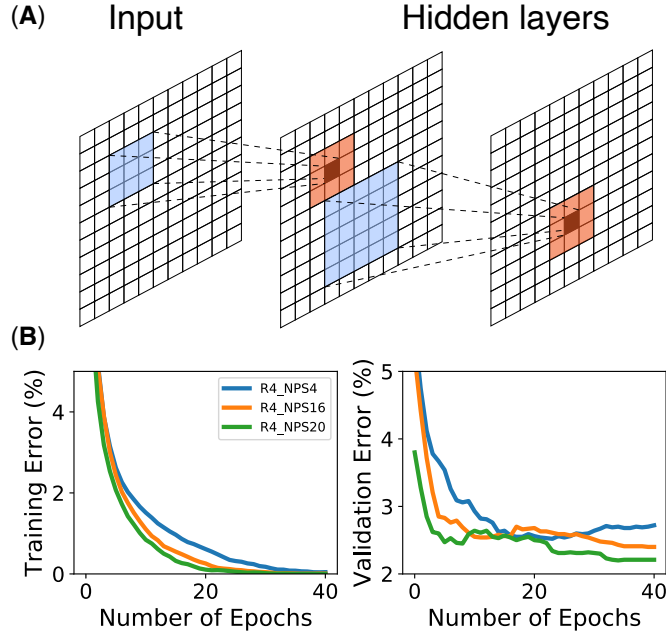


Figure 6: (A) Sketch of structured connectivity in a deep neural network. Neurons live on a 2-d grid. Each neuron takes input from a small grid (blue shades) from the previous layer and a small grid of inhibition from its nearby neurons (orange shades). (B) Training and validation curves of CSM with structured single hidden layer networks on MNIST dataset, with a receptive field of radius 4 and neurons per site 4, 16, and 20.

to rhythms in the brain. In more recent work, [Scellier and Bengio \(2017\)](#) provided an implementation of EP also applicable to CSM with minor modifications. They proposed that synaptic update only happens in the nudged phase with weights continuously updating according to a differential anti-Hebbian rule as the neuron’s state moves from the fixed point at free phase to the fixed point at the nudged phase. Further, such differential rule can be related to spike time dependent plasticity ([Xie and Seung, 2000](#); [Bengio et al., 2015](#)). CSM can use the same mechanism for feedforward and feedback updates. Lateral connections need to be separately updated in the free phase. The differential updating of synapses in different phases of the algorithm can be implemented by neuromodulatory gating of synaptic plasticity ([Brzosko et al., 2019](#); [Bazzari and Parri, 2019](#)).

A practical issue of CSM and other energy-based algorithms such as EP and CHL is that the recurrent dynamics takes a long time to converge. Recently, a discrete-time version of EP has shown much faster training speed ([Ernault et al., 2019](#)) and the application to the CSM could be an interesting future direction.

Acknowledgements

We acknowledge support by NIH, the Intel Corporation through Intel Neuromorphic Research Community, and a Google Faculty Research Award. We thank Dina Obeid and Blake Bordelon for helpful discussions.

A Derivation of a Supervised Similarity Matching Neural Network

The supervised similarity matching cost function (1) is formulated in terms of the activities of units, but a statement about the architecture and the dynamics of the network has not been made. We will derive all these from the cost function, without prescribing them. To do so, we need to introduce variables that correspond to the synaptic weights in the network. As it turns out, these variables are dual to correlations between unit activities (Pehlevan et al., 2018).

To see this explicitly, following the method of (Pehlevan et al., 2018), we expand the squares in Eq.(1) and introduce new dual variables $\mathbf{W}_1 \in \mathbb{R}^{m \times n}$, $\mathbf{W}_2 \in \mathbb{R}^{k \times m}$ and $\mathbf{L}_1 \in \mathbb{R}^{m \times m}$ using the following identities:

$$\begin{aligned}
 -\frac{1}{T^2} \sum_{t=1}^T \sum_{t'=1}^T \mathbf{y}_t^\top \mathbf{y}_{t'} \mathbf{x}_t^\top \mathbf{x}_{t'} &= \min_{\mathbf{W}_1} -\frac{2}{T} \sum_{t=1}^T \mathbf{y}_t^\top \mathbf{W}_1 \mathbf{x}_t + \text{Tr} \mathbf{W}_1^\top \mathbf{W}_1, \\
 \frac{1}{T^2} \sum_{t=1}^T \sum_{t'=1}^T \mathbf{y}_t^\top \mathbf{y}_{t'} \mathbf{y}_t^\top \mathbf{y}_{t'} &= \max_{\mathbf{L}_1} \frac{2}{T} \sum_{t=1}^T \mathbf{y}_t^\top \mathbf{L}_1 \mathbf{y}_t - \text{Tr} \mathbf{L}_1^\top \mathbf{L}_1, \\
 -\frac{1}{T^2} \sum_{t=1}^T \sum_{t'=1}^T \mathbf{y}_t^\top \mathbf{y}_{t'} \mathbf{z}_t^{l^\top} \mathbf{z}_{t'}^l &= \min_{\mathbf{W}_2} -\frac{2}{T} \sum_{t=1}^T \mathbf{z}_t^{l^\top} \mathbf{W}_2 \mathbf{y}_t + \text{Tr} \mathbf{W}_2^\top \mathbf{W}_2. \tag{14}
 \end{aligned}$$

Plugging these into Eq.(1), and changing orders of optimization, we arrive the following dual, minimax formulation of supervised similarity matching:

$$\min_{\mathbf{W}_1, \mathbf{W}_2} \max_{\mathbf{L}_1} \frac{1}{T} \sum_{t=1}^T l_t(\mathbf{W}_1, \mathbf{W}_2, \mathbf{L}_1, \mathbf{x}_t, \mathbf{z}_t^l), \tag{15}$$

where

$$\begin{aligned}
 l_t &:= \text{Tr} \mathbf{W}_1^\top \mathbf{W}_1 - \text{Tr} \mathbf{L}_1^\top \mathbf{L}_1 + \text{Tr} \mathbf{W}_2^\top \mathbf{W}_2 \\
 &\quad + \min_{\mathbf{y}_t} 2(-\mathbf{y}_t^\top \mathbf{W}_1 \mathbf{x}_t + \mathbf{y}_t^\top \mathbf{L}_1 \mathbf{y}_t - \mathbf{y}_t^\top \mathbf{W}_2^\top \mathbf{z}_t^l). \tag{16}
 \end{aligned}$$

A stochastic optimization of the above objective can be mapped to a Hebbian/anti-Hebbian network following steps in (Pehlevan et al., 2018). For each training datum, $\{\mathbf{x}_t, \mathbf{z}_t^l\}$, a two-step procedure is performed. First, optimal \mathbf{y}_t that minimizes l_t is obtained by a gradient flow until convergence,

$$\dot{\mathbf{y}} = \mathbf{W}_1 \mathbf{x}_t - 2\mathbf{L}_1 \mathbf{y}_t + \mathbf{W}_2^\top \mathbf{z}_t^l. \tag{17}$$

We interpret this flow as the dynamics of a neural circuit with linear activation functions, where the dual variables \mathbf{W}_1 , \mathbf{W}_2 and \mathbf{L}_1 are synaptic weight matrices

(Fig. 7A). In the second part of the algorithm, we update the synaptic weights by a gradient descent-ascent on (16) with \mathbf{y}_t fixed. This gives the following synaptic plasticity rules

$$\Delta \mathbf{W}_1 = \eta(\mathbf{y}_t \mathbf{x}_t^\top - \mathbf{W}_1), \quad \Delta \mathbf{L}_1 = \eta(\mathbf{y}_t \mathbf{y}_t^\top - \mathbf{L}_1), \quad \Delta \mathbf{W}_2 = \eta(\mathbf{z}_t^l \mathbf{y}_t^\top - \mathbf{W}_2). \quad (18)$$

The learning rate η of each matrix can be chosen differently to achieve best performance.

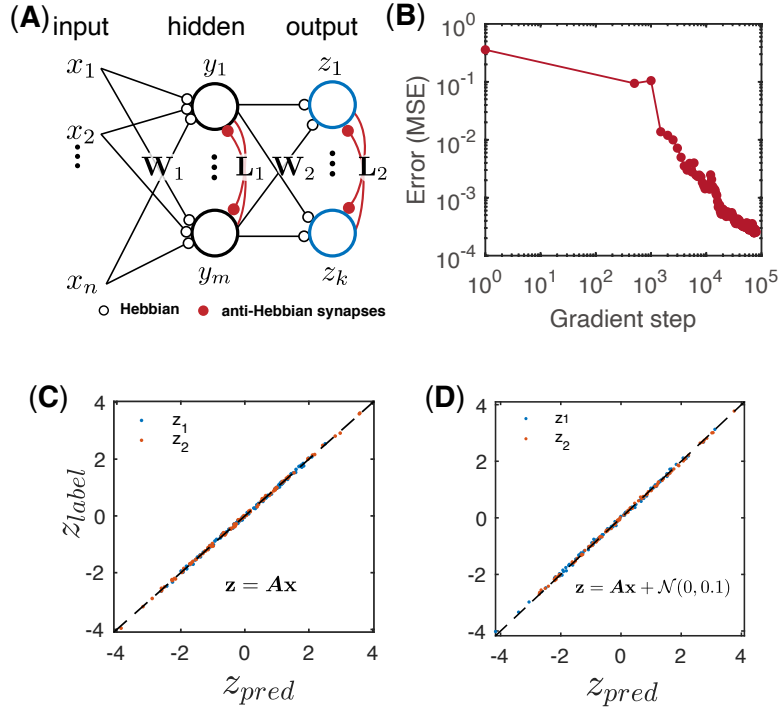


Figure 7: A linear NN with Hebbian/anti-Hebbian learning rules. (A) During the learning process, the output neurons (blue) are clamped at their desired states. After training, prediction for a new input \mathbf{x} is given by the value of \mathbf{z} at the fixed point of neural dynamics. (B) The network is trained on a linear task: $\mathbf{z}_t^l = \mathbf{A}\mathbf{x}_t$. Test error, defined as the mean square error between the network’s prediction, \mathbf{z}_t^p , and the ground-truth value, \mathbf{z}_t^l , $1/T \sum_{t=1}^T \|\mathbf{z}_t^p - \mathbf{z}_t^l\|_F^2$, decreases with the gradient ascent-descent steps during learning. (C) Scatter plot of the predicted value versus the desired value (element-wise). (D) The algorithm learns the correct mapping between \mathbf{x} and \mathbf{z} even in the presence of small Gaussian noise. In these examples, $\mathbf{x} \in \mathbb{R}^5$, $\mathbf{A} \in \mathbb{R}^{2 \times 5}$, elements of \mathbf{x} and \mathbf{A} are drawn from a uniform distribution in the range $[-1, 1]$, $\mathbf{y} \in \mathbb{R}^2$ and $\mathbf{z} \in \mathbb{R}^2$. In (C) and (D), 200 data points are shown.

Overall, the network dynamics (17) and the update rules (18) map to a NN with one hidden layer, with the output layer clamped to the desired state. The

updates of the feedforward weight are Hebbian, and updates of the lateral weight are anti-Hebbian (Fig. 7A).

For prediction, the network takes an input data point, \mathbf{x}_t , and runs with unclamped output until convergence. We take the value of the \mathbf{z} units at the fixed point as the network’s prediction.

Because the \mathbf{z} units are not clamped during prediction and are dynamical variables, the correct outputs are not necessarily the fixed points of the network in the prediction phase. To make sure that the network produces correct fixed points, at least for training data, we introduce the following step to the training procedure. We aim to construct a neural dynamics for the output layer in prediction phase such that its fixed point \mathbf{z} corresponds to the desired output \mathbf{z}^l . Since the output layer receives input $\mathbf{W}_2\mathbf{y}$ from the previous layer, a decay term that depends on \mathbf{z} is required to achieve stable fixed point at $\mathbf{z} = \mathbf{z}^l$. The simplest way is introducing lateral inhibition. And now the output layer has the following neural dynamics:

$$\dot{\mathbf{z}} = \mathbf{W}_2\mathbf{y} - \mathbf{L}_2\mathbf{z}, \quad (19)$$

where the lateral connections \mathbf{L}_2 are learned such that the fixed point $\mathbf{z}^* \approx \mathbf{z}^l$. This is achieved by minimizing the following target function

$$\min_{\mathbf{L}_2} \frac{1}{T} \sum_{t=1}^T \|\mathbf{W}_2\mathbf{y}_t - \mathbf{L}_2\mathbf{z}_t^l\|_2^2. \quad (20)$$

Taking the derivative of the above target function with respect to \mathbf{L}_2 while keeping the other parameters and variables evaluated at the fixed point of neural dynamics, we get the following “delta” learning rule for \mathbf{L}_2 :

$$\Delta\mathbf{L}_2 = \eta(\mathbf{W}_2\mathbf{y}_t - \mathbf{L}_2\mathbf{z}_t^l)\mathbf{z}_t^{l\top}. \quad (21)$$

After learning, the NN makes a prediction about a new input \mathbf{x} by running the neural dynamics of \mathbf{y} and \mathbf{z} (17) and (19) until they converge to a fixed point. We take the value of \mathbf{z} units at the fixed point as the prediction. As shown in Fig.7 B-D, the linear network and weight update rule solve linear tasks efficiently.

Although the above procedure can be generalized to multi-layer and nonlinear networks, one has to address the issue of spurious fixed points of nonlinear dynamics for a given input \mathbf{x}_t . The Contrastive Similarity Matching algorithm presented in the main text overcome this problem, which borrows ideas from energy-based learning algorithms such as Contrastive Hebbian Learning and Equilibrium Propagation.

B Supervised Deep Similarity Matching

In this section, we follow (Obeid et al., 2019) to derive the minimax dual of deep similarity matching objective function. We start from rewriting the objective func-

tion (3) by expanding its first term and combining the same terms from adjacent layers, which gives

$$\begin{aligned} & \min_{\substack{a_1 \leq \mathbf{r}_t^p \leq a_2 \\ t=1, \dots, T \\ p=1, \dots, P}} \sum_{p=1}^P \frac{\gamma^{p-P}}{2T^2} \sum_{t=1}^T \sum_{t'=1}^T \left(\mathbf{r}_t^{(p)\top} \mathbf{r}_{t'}^{(p)} \mathbf{r}_t^{(p-1)\top} \mathbf{r}_{t'}^{(p-1)} - \frac{1 + \gamma(1 - \delta_{pP})}{2} c^{(p)} \mathbf{r}_t^{(p)\top} \mathbf{r}_{t'}^{(p)} \mathbf{r}_t^{(p)\top} \mathbf{r}_{t'}^{(p)} \right) \\ & + \sum_{p=1}^P \frac{2\gamma^{p-P}}{T} \sum_{t=1}^T \mathbf{F}(\mathbf{r}_t^{(p)})^\top \mathbf{1} + \frac{\beta}{T} \sum_{t=1}^T \left\| \mathbf{r}_t^{(P)} - \mathbf{z}_t^l \right\|_2^2, \end{aligned} \quad (22)$$

where $c^{(p)}$ is a parameter that change the relative importance of within-layer and between-layer similarity, we set it to be 1/2 in our numerical simulations. Plug the following identities:

$$-\frac{1}{T^2} \sum_{t=1}^T \sum_{t'=1}^T \mathbf{r}_t^{(p)\top} \mathbf{r}_{t'}^{(p)} \mathbf{r}_t^{(p-1)\top} \mathbf{r}_{t'}^{(p-1)} = \min_{\mathbf{W}^{(p)}} -\frac{2}{T} \sum_{t=1}^T \mathbf{r}_t^{(p)\top} \mathbf{W}^{(p)} \mathbf{r}_t^{(p-1)} + \text{Tr} \mathbf{W}^{(p)\top} \mathbf{W}^{(p)}, \quad (23)$$

$$\frac{1}{T^2} \sum_{t=1}^T \sum_{t'=1}^T \mathbf{r}_t^{(p)\top} \mathbf{r}_{t'}^{(p)} \mathbf{r}_t^{(p)\top} \mathbf{r}_{t'}^{(p)} = \max_{\mathbf{L}^{(p)}} \frac{2}{T} \sum_{t=1}^T \mathbf{r}_t^{(p)\top} \mathbf{L}^{(p)} \mathbf{r}_t^{(p)} - \text{Tr} \mathbf{L}^{(p)\top} \mathbf{L}^{(p)}, \quad (24)$$

in (22) and exchange the optimization order of $\mathbf{r}_t^{(p)}$ and the weight matrices, we turn the target function (3) into the following minmax problem

$$\min_{\{\mathbf{W}^{(p)}\}} \max_{\{\mathbf{L}^{(p)}\}} \frac{1}{T} \sum_{t=1}^T l_t \left(\{\mathbf{W}^{(p)}\}, \{\mathbf{L}^{(p)}\}, \mathbf{r}_t^{(0)}, \mathbf{z}_t^l, \beta \right), \quad (25)$$

where we have defined an ‘‘energy’’ term (Eq.5 in the main text). The neural dynamics of each layer can be derived by following the gradient of l_t :

$$\begin{aligned} \frac{d\mathbf{u}_t^{(p)}}{dt} & \propto -\frac{\partial l_t}{\partial \mathbf{r}_t^{(p)}} = 2\gamma^{p-P} \left[-\mathbf{u}^{(p)} + \mathbf{b}_t^{(p)} + \mathbf{W}^{(p)} \mathbf{r}_t^{(p-1)} + \gamma(1 - \delta_{pP}) \mathbf{W}^{(p+1)\top} \mathbf{r}_t^{(p+1)} \right. \\ & \quad \left. - [1 + \gamma(1 - \delta_{pP})] c^{(p)} \mathbf{L}^{(p)} \mathbf{r}_t^{(p)} - 2\beta \delta_{pP} (\mathbf{r}_t^{(P)} - \mathbf{z}_t^l) \right], \\ \mathbf{r}_t^{(p)} & = \mathbf{f}(\mathbf{u}^{(p)}). \end{aligned} \quad (26)$$

Define $\tau_p^{-1} = 2\gamma^{p-P}$, the above equation becomes Eq.6 in the main text.

C Supervised Similarity Matching for Neural Networks with Structured Connectivity

In this section, we derive the supervised similarity matching algorithm for neural networks with structured connectivity. Structure can be introduced to the quartic terms in (22):

$$\begin{aligned}
& - \frac{1}{T^2} \sum_i^{N^{(p)}} \sum_j^{N^{(p-1)}} \sum_t^T \sum_{t'}^T r_{t,i}^{(p)} r_{t',i}^{(p)} r_{t,j}^{(p-1)} r_{t',j}^{(p-1)} s_{ij}^{W,(p)}, \\
& - \frac{1}{T^2} \sum_i^{N^{(p)}} \sum_j^{N^{(p)}} \sum_t^T \sum_{t'}^T r_{t,i}^{(p)} r_{t',i}^{(p)} r_{t,j}^{(p)} r_{t',j}^{(p)} s_{ij}^{L,(p)},
\end{aligned} \tag{27}$$

where $s_{ij}^{W,(p)}$ and $s_{ij}^{L,(p)}$ specify the feedforward connections of layer p with p-1 layer and lateral connections within layer p respectively. For example, setting them to be 0s eliminates all connections. Now we have the following deep structured similarity matching cost function for supervised learning:

$$\begin{aligned}
& \min_{\substack{a_1 \leq \mathbf{r}_t^p \leq a_2 \\ t=1, \dots, T \\ p=1, \dots, P}} \sum_{p=1}^P \frac{\gamma^{p-P}}{2T^2} \sum_{t=1}^T \sum_{t'=1}^T \left(\mathbf{r}_t^{(p)\top} \mathbf{r}_{t'}^{(p)} \mathbf{r}_t^{(p-1)\top} \mathbf{r}_{t'}^{(p-1)} s_{ij}^{W,(p)} - \frac{1 + \gamma(1 - \delta_{pP})}{2} \mathbf{r}_t^{(p)\top} \mathbf{r}_{t'}^{(p)} \mathbf{r}_t^{(p)\top} \mathbf{r}_{t'}^{(p)} s_{ij}^{L,(p)} \right) \\
& + \sum_{i=1}^P \frac{2\gamma^{p-P}}{T} \sum_{t=1}^T \mathbf{F}(\mathbf{r}_t^{(p)})^\top \mathbf{1} + \frac{\beta}{T} \sum_{t=1}^T \left\| \mathbf{r}_t^{(P)} - \mathbf{z}_t^l \right\|_2^2.
\end{aligned} \tag{28}$$

For each layer, we can define dual variables for $\mathbf{W}_{ij}^{(p)}$ and $\mathbf{L}_{ij}^{(p)}$ for interactions with positive constants, and define the following variables

$$\bar{W}_{ij}^{(p)} = \begin{cases} W_{ij}^{(p)}, & s_{ij}^{W,(p)} \neq 0 \\ 0, & s_{ij}^{W,(p)} = 0 \end{cases}, \quad \bar{L}_{ij}^{(p)} = \begin{cases} L_{ij}^{(p)}, & s_{ij}^{L,(p)} \neq 0 \\ 0, & s_{ij}^{L,(p)} = 0 \end{cases} \tag{29}$$

Now we can rewrite (28) as:

$$\min_{\{\bar{\mathbf{W}}^{(p)}\}} \max_{\{\bar{\mathbf{L}}^{(p)}\}} \frac{1}{T} \sum_{t=1}^T \bar{l}_t \left(\{\bar{\mathbf{W}}^{(p)}\}, \{\bar{\mathbf{L}}^{(p)}\}, \mathbf{r}_t^{(0)}, \mathbf{z}_t^l, \beta \right), \tag{30}$$

where

$$\bar{l}_t := \min_{\substack{a_1 \leq \mathbf{r}_t^{(p)} \leq a_2 \\ p=1, \dots, P}} \sum_{p=1}^P \gamma^{p-P} \left\{ \sum_{\substack{i,j \\ s_{ij}^{W,(p)} \neq 0}} W_{ij}^{(p)2} - \sum_{\substack{i,j \\ s_{ij}^{L,(p)} \neq 0}} \frac{1 + \gamma(1 - \delta_{pP})}{s_{ij}^{L,(p)}} L_{ij}^{(p)2} + \right. \\ \left. [1 + \gamma(1 - \delta_{pP})] \mathbf{r}_t^{(p)} \mathbf{L}^{(p)} \mathbf{r}_t^{(p)} - 2\mathbf{r}_t^{(p)\top} \mathbf{W}^{(p)} \mathbf{r}_t^{(p-1)} + 2\mathbf{F} \left(\mathbf{r}_t^{(p)} \right)^\top \right\} + \beta \left\| \mathbf{r}_t^{(P)} - \mathbf{z}_t^l \right\|_2^2. \quad (31)$$

The neural dynamics follows the gradient of (31), which is

$$\tau_p \frac{d\mathbf{u}_t^{(p)}}{dt} = -\mathbf{u}^{(p)} + \mathbf{b}_t^{(p)} + \bar{\mathbf{W}}^{(p)} \mathbf{r}_t^{(p-1)} + \gamma(1 - \delta_{pP}) \bar{\mathbf{W}}^{(p+1)\top} \mathbf{r}_t^{(p+1)} \\ - [1 + \gamma(1 - \delta_{pP})] \bar{\mathbf{L}}^{(p)} \mathbf{r}_t^{(p)} - \beta \delta_{pP} (\mathbf{r}_t^{(P)} - \mathbf{z}_t^l), \\ \mathbf{r}_t^{(p)} = \mathbf{f}(\mathbf{u}^{(p)}), \quad p = 1, \dots, P. \quad (32)$$

Local learning rules follow the gradient descent and ascent of (31):

$$\Delta W_{ij}^{(p)} \propto \left(r_j^{(p)} r_i^{(p-1)} - \frac{W_{ij}^{(p)}}{s_{ij}^{W,(p)}} \right), \quad (33)$$

$$\Delta L_{ij}^{(p)} \propto \left(r_j^{(p)} r_i^{(p)} - \frac{L_{ij}^{(p)}}{s_{ij}^{L,(p)}} \right). \quad (34)$$

D Hyperparameters and Performance in Numerical Simulations with the MNIST Dataset

D.1 One Hidden Layer

Table 2 reports the training and validation errors of three variants of the EP algorithm and the CSM algorithm for a single hidden layer network on MNIST. The models were trained until the training error dropped to 0% or as close to 0% as possible (as in the case of EP algorithm with $\beta > 0$); errors reported herein correspond to errors obtained for specific runs and do not reflect ensemble averages. The training and validation errors below, and in subsequent subsections are reported at an epoch when the training error has dropped to 0%, or at the last epoch for the run (eg. for EP $\beta > 0$). This epoch number is recorded in the last column.

Table 2: Comparison of the training and validation errors of different algorithms for one hidden layer NNs on MNIST data set

ALGORITHM	LEARNING RATE	TRAINING ERROR (%)	VALIDATION ERROR (%)	NO. EPOCHS
EP: $\pm\beta$	$\alpha_W = 0.1, 0.05$	0	2.53	40
EP: $+\beta$	$\alpha_W = 0.5, 0.125$	0.034	2.18	100
EP: LATERAL	$\alpha_W = 0.5, 0.25, \alpha_L$ $= 0.75$	0	2.29	25
CSM	$\alpha_W = 0.5, 0.375,$ $\alpha_L = 0.01$	0	2.16	25

D.2 Three Hidden Layers

In Table 3, the CSM algorithm employs a scheme with decaying learning rates. Specifically, the learning rates for lateral updates are divided by a factor of 5, 10, 50, and 100 when the training error dropped below 5%, 1%, 0.5%, and 0.1% respectively.

Table 3: Comparison of the training and validation errors of different algorithms for three hidden layer NNs on MNIST data set

ALGORITHM	LEARNING RATE	TRAINING ERROR (%)	VALIDATION ERROR (%)	NO. EPOCHS
EP: $\pm\beta$	$\alpha_W=0.128, 0.032, 0.008, 0.002$	0	2.73	250
EP: $+\beta$	$\alpha_W =0.128, 0.032, 0.008, 0.002$	0	2.77	250
EP LATERAL	$\alpha_W=0.128, 0.032, 0.008, 0.002;$ $\alpha_L = 0.192, 0.048, 0.012$	0	2.4	250
CSM	$\alpha_W =0.5, 0.375, 0.281, 0.211;$ $\alpha_L =0.75, 0.562, 0.422$	0	4.82	250
CSM ADAP- TIVE	$\alpha_W =0.5, 0.375, 0.281, 0.211;$ $\alpha_L =0.75, 0.562, 0.422$	0	3.52	250

D.3 Structured Connectivity

In this section, we explain the simulation for structured connectivity and report the results. Every hidden layer in these networks can be considered as multiple two dimensional grids stacked onto each other, with each grid containing neurons/units at periodically arranged sites. Each site only receives inputs from selected nearby sites. In this scheme, we consider lateral connections only between neurons sharing the same (x, y) coordinate, and the length and width of the grid are the same. In Table 4, ‘Full’ refers to simulations where the input is the 28×28 MNIST input image and ‘Crop’ refers to simulations in which the input image is a cropped 20×20 MNIST image. The first three, annotated by ‘Full’, correspond to the simulations reported in the main text. Errors are reported at the last epoch for the run. In networks with structural connectivity, additional hyperparameters are required to constrain the structure, which are enumerated below:

- Neurons-per-site (nps): The number of neurons placed at each site in a given hidden layer, i.e. the number of two dimensional grids stacked onto each other. The nps for the input is 1.
- Stride: Spacing between adjacent sites, relative to the input channel. The stride of the input is always 1, i.e. sites are placed at $(0, 0)$, $(0, 1)$, $(1, 0)$, so on, on the two dimensional grid. If the stride of the l -th layer is s , the nearest sites to the site at the origin will be $(0, s)$ and $(s, 0)$. The stride increases deeper into the network. Specifying the stride also determines the dimension of the grid. A layer with stride s and nps n , will have $d \times d \times n$ units, where $d = 28/s$ for the ‘Full’ runs and $d = 20/s$ for the ‘Crop’ runs. The nps values and stride together assign coordinates to all the units in the network.
- Radius: The radius of the circular two-dimensional region that all units in the previous layer must lie within in order to have non-zero weights to the current unit. Any units in the previous layer, lying outside the circle will not be connected to the unit.

Table 4: Comparison of the training and validation errors of different algorithms for one hidden layer NNs with structured connectivity on MNIST data set

ALGORITHM	LEARNING RATE	TRAINING ERROR (%)	VALIDATION ERROR (%)	No. EPOCHS
R4, NPS4, FULL	$\alpha_W = 0.5, 0.375;$ $\alpha_L = 0.01$	0.02	2.71	50
R4, NPS16, FULL	$\alpha_W = 0.5, 0.25;$ $\alpha_L = 0.75$	0	2.41	49
R4, NPS20, FULL	$\alpha_W = 0.664, 0.577;$ $\alpha_L = 0.9$	0	2.22	50
R8, NPS80, CROP	$\alpha_W = 0.664, 0.577;$ $\alpha_L = 0.9$	0.01	2.27	20
R4, NPS4, CROP	$\alpha_W = 0.099, 0.065;$ $\alpha_L = 0.335$	0.08	2.98	100
R8, NPS4, CROP	$\alpha_W = 0.099, 0.065;$ $\alpha_L = 0.335$	0	2.73	100
R8, NPS20, CROP	$\alpha_W = 0.664, 0.577;$ $\alpha_L = 0.9$	0	2.23	79

E Hyperparameters and Performance in Numerical Simulations with the CIFAR-10 Dataset

Table 5 records the training and validation errors obtained for the CSM and EP algorithms for fully connected networks, as well as for CSM with structured networks, on the CIFAR-10 dataset. The validation error column for fully connected runs reports the mean of the last twenty validation errors reported at the end of the training period as well as the standard error on the mean. For the structured runs, the training and validation errors reported are the average of the last epoch’s reported errors from 5 trials and the standard error on the means. This is done in order to account for fluctuations in the error during training.

F Performance of CSM as a Function of Nudge Strength and Feedback Strength

In the nudged deep similarity matching objective (3), β controls the strength of nudging, while γ specifies the strength of feedback input compared with the

Table 5: Comparison of the validation errors of different algorithms for different networks.

ALGORITHM, CONNECTIVITY, NO. HIDDEN LAYERS	LEARNING RATE	TRAIN ERROR (%)	VAL ERROR (%)	NO. EPOCHS
CSM, FC, 1HL	$\alpha_W = 0.059, 0.017$ $\alpha_L = 0.067$	1.77	59.21 ± 0.08	1000
CSM, FC, 2HL	$\alpha_W =$ $0.018, 7.51 \times 10^{-4}, 3.07 \times 10^{-5}$ $\alpha_L = 0.063, 2.59 \times 10^{-3}$	17.96	51.76 ± 0.002	3584
CSM, STR, 1HL	$\alpha_W = 0.050, 0.0375$ $\alpha_L = 0.01$	34 ± 3.7	49.5 ± 0.7	250
CSM, STR, 2HL	$\alpha_W = 0.265, 0.073, 0.020$ $\alpha_L = 0.075, 0.020$	$46.8 \pm$ 0.6	51.4 ± 0.7	200
EP, FC, 1HL	$\alpha_W = 0.014, 0.011$	0.76	57.60 ± 0.06	1000
EP, FC, 2HL	$\alpha_W = 0.014, 0.011, 1.25$	1.25	53.43 ± 0.04	1000

feedforward input. Scellier and Bengio (2017) used $\beta = 1$ in their simulations. In all the simulations reported here in the main text, we have set $\beta = 1, \gamma = 1$. In this section, we trained a single hidden layer network using CSM on MNIST, while systematically varying the value of β and γ and keeping other parameters fixed. The validation errors for these experiments are documented in Table 6 and 7 and plotted in Fig.8. We find that the network has optimal values for γ less than 1.5, and β in the range bounded by 0.5 and 1. At these values, the network is able to converge to low validation errors ($< 3\%$).

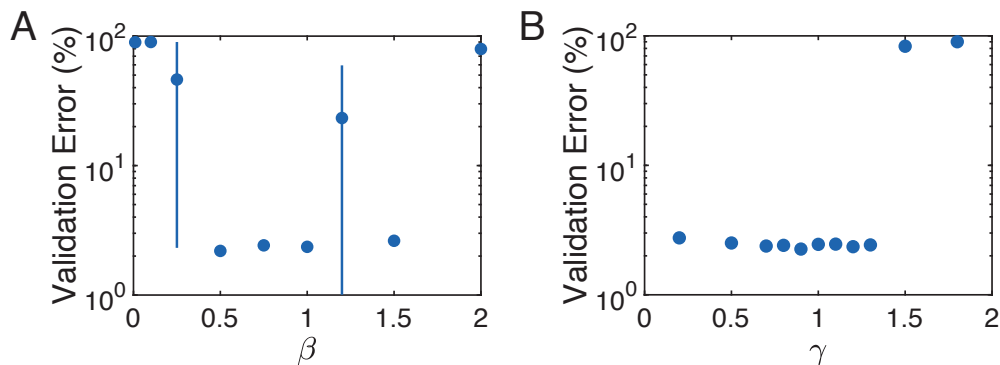


Figure 8: Validation error of a single hidden layer network trained by CSM algorithm on MNIST dataset as a function of parameter β (A) and γ (B). 4 trials were conducted for values for which the validation error was less than 3%. Dots indicate the mean validation error over trials, and errorbars indicate the standard deviation over trials.

Table 6: Validation errors at the end of the training period for a fully connected 1 hidden layer network trained on MNIST, with different β values. For values that lay within the parameter range that converged to low ($< 3\%$) validation errors, 4 trials were run, and the mean, minimum and maximum errors over the trials have been reported. In all runs, $\gamma = 1$.

β VALUE	MEAN VALIDATION ERROR (%)	MINIMUM VALIDATION ERROR (%)	MAXIMUM VALIDATION ERROR (%)
0.01	89.70	89.70	89.70
0.1	90.09	90.09	90.09
0.25	46.20	2.28	90.09
0.5	2.19	2.17	2.21
0.75	2.42	2.22	2.51
1.0	2.36	2.26	2.48
1.2	23.30	2.36	85.91
1.5	2.62	2.40	2.75
2.0	79.55	79.55	79.55

Table 7: Validation errors at the end of the training period for a fully connected 1 hidden layer network trained on MNIST, with different γ values. For parameters that converged to low ($< 3\%$) validation errors, 4 trials were run, and the mean, minimum and maximum errors over the trials have been reported. In all runs, $\beta = 1$.

γ VALUE	MEAN VALIDATION ERROR (%)	MINIMUM VALIDATION ERROR (%)	MAXIMUM VALIDATION ERROR (%)
0.2	2.75	2.64	2.85
0.5	2.51	2.43	2.60
0.7	2.38	2.24	2.47
0.8	2.41	2.32	2.47
0.9	2.26	2.21	2.31
1.0	2.45	2.38	2.53
1.1	2.46	2.37	2.63
1.2	2.35	2.26	2.48
1.3	2.43	2.28	2.54
1.5	83.16	83.16	83.16
1.8	90.09	90.09	90.09

References

- Anderson, J. R. and Peterson, C. (1987). A mean field theory learning algorithm for neural networks. *Complex Systems*, 1:995–1019.
- Baldi, P. and Pineda, F. (1991). Contrastive learning and neural oscillations. *Neural Computation*, 3(4):526–545.
- Bazzari, A. H. and Parri, H. R. (2019). Neuromodulators and long-term synaptic plasticity in learning and memory: A steered-glutamatergic perspective. *Brain sciences*, 9(11):300.
- Belilovsky, E., Eickenberg, M., and Oyallon, E. (2018). Greedy layerwise learning can scale to imagenet. *arXiv preprint [arXiv:1812.11446](https://arxiv.org/abs/1812.11446)*.
- Bengio, Y., Mesnard, T., Fischer, A., Zhang, S., and Wu, Y. (2015). Stdp as presynaptic activity times rate of change of postsynaptic activity. *arXiv preprint [arXiv:1509.05936](https://arxiv.org/abs/1509.05936)*.
- Brzosko, Z., Mierau, S. B., and Paulsen, O. (2019). Neuromodulation of spike-timing-dependent plasticity: past, present, and future. *Neuron*, 103(4):563–581.
- Crick, F. (1989). The recent excitement about neural networks. *Nature*, 337(6203):129–132.
- Ernault, M., Grollier, J., Querlioz, D., Bengio, Y., and Scellier, B. (2019). Updates of equilibrium prop match gradients of backprop through time in an rnn with static input. In *Advances in Neural Information Processing Systems*, pages 7079–7089.
- Genkin, A., Sengupta, A. M., and Chklovskii, D. (2019). A neural network for semi-supervised learning on manifolds. In *International Conference on Artificial Neural Networks*, pages 375–386. Springer.
- Grill-Spector, K. and Weiner, K. S. (2014). The functional architecture of the ventral temporal cortex and its role in categorization. *Nature Reviews Neuroscience*, 15(8):536–548.
- Guerguiev, J., Lillicrap, T. P., and Richards, B. A. (2017). Towards deep learning with segregated dendrites. *ELife*, 6:e22901.
- Hinton, G. E. and McClelland, J. L. (1988). Learning representations by recirculation. In *Neural information processing systems*, pages 358–366.

- Kandel, E. R., Schwartz, J. H., Jessell, T. M., of Biochemistry, D., Jessell, M. B. T., Siegelbaum, S., and Hudspeth, A. (2000). *Principles of neural science*, volume 4. McGraw-hill New York.
- Kriegeskorte, N., Mur, M., Ruff, D. A., Kiani, R., Bodurka, J., Esteky, H., Tanaka, K., and Bandettini, P. A. (2008). Matching categorical object representations in inferior temporal cortex of man and monkey. *Neuron*, 60(6):1126–1141.
- Krizhevsky, A., Hinton, G., et al. (2009). Learning multiple layers of features from tiny images.
- LeCun, Y., Cortes, C., and Burges, C. (2010). Mnist handwritten digit database. *ATT Labs [Online]*. Available: <http://yann.lecun.com/exdb/mnist>, 2.
- Lee, D.-H., Zhang, S., Fischer, A., and Bengio, Y. (2015). Difference target propagation. In *Joint European Conference on Machine Learning and Knowledge Discovery in Databases*, pages 498–515. Springer.
- Li, Z., Brendel, W., Walker, E., Cobos, E., Muhammad, T., Reimer, J., Bethge, M., Sinz, F., Pitkow, Z., and Tolias, A. (2019). Learning from brains how to regularize machines. In *Advances in Neural Information Processing Systems*, pages 9525–9535.
- Lillicrap, T. P., Cownden, D., Tweed, D. B., and Akerman, C. J. (2016). Random synaptic feedback weights support error backpropagation for deep learning. *Nature Communications*, 7:13276.
- Lillicrap, T. P., Santoro, A., Marris, L., Akerman, C. J., and Hinton, G. (2020). Backpropagation and the brain. *Nature Reviews Neuroscience*, pages 1–12.
- Movellan, J. R. (1991). Contrastive hebbian learning in the continuous hopfield model. In *Connectionist models*, pages 10–17. Elsevier.
- Nøkland, A. (2016). Direct feedback alignment provides learning in deep neural networks. In *Advances in Neural Information Processing Systems*, pages 1037–1045.
- Nøkland, A. and Eidnes, L. H. (2019). Training neural networks with local error signals. *arXiv preprint [arXiv:1901.06656](https://arxiv.org/abs/1901.06656)*.
- Obeid, D., Ramambason, H., and Pehlevan, C. (2019). Structured and deep similarity matching via structured and deep hebbian networks. In *Advances in Neural Information Processing Systems*, pages 15377–15386.

- Olshausen, B. A. and Field, D. J. (2004). Sparse coding of sensory inputs. *Current opinion in neurobiology*, 14(4):481–487.
- Ororbia, A. G. and Mali, A. (2019). Biologically motivated algorithms for propagating local target representations. In *Proceedings of the AAAI Conference on Artificial Intelligence*, volume 33, pages 4651–4658.
- Pehlevan, C. and Chklovskii, D. (2015). A normative theory of adaptive dimensionality reduction in neural networks. In *Advances in neural information processing systems*, pages 2269–2277.
- Pehlevan, C. and Chklovskii, D. B. (2019). Neuroscience-inspired online unsupervised learning algorithms: Artificial neural networks. *IEEE Signal Processing Magazine*, 36(6):88–96.
- Pehlevan, C., Mohan, S., and Chklovskii, D. B. (2017). Blind nonnegative source separation using biological neural networks. *Neural computation*, 29(11):2925–2954.
- Pehlevan, C., Sengupta, A. M., and Chklovskii, D. B. (2018). Why do similarity matching objectives lead to hebbian/anti-hebbian networks? *Neural computation*, 30(1):84–124.
- Richards, B. A. and Lillicrap, T. P. (2019). Dendritic solutions to the credit assignment problem. *Current Opinion in Neurobiology*, 54:28–36.
- Rumelhart, D. E., Hinton, G. E., and Williams, R. J. (1986). Learning representations by back-propagating errors. *nature*, 323(6088):533–536.
- Sacramento, J., Costa, R. P., Bengio, Y., and Senn, W. (2018). Dendritic cortical microcircuits approximate the backpropagation algorithm. In *Advances in Neural Information Processing Systems*, pages 8721–8732.
- Scellier, B. and Bengio, Y. (2017). Equilibrium propagation: Bridging the gap between energy-based models and backpropagation. *Frontiers in computational neuroscience*, 11:24.
- Sengupta, A., Pehlevan, C., Tepper, M., Genkin, A., and Chklovskii, D. (2018). Manifold-tiling localized receptive fields are optimal in similarity-preserving neural networks. In *Advances in Neural Information Processing Systems*, pages 7080–7090.
- Team, T. T. D., Al-Rfou, R., Alain, G., Almahairi, A., Angermueller, C., Bahdanau, D., Ballas, N., Bastien, F., Bayer, J., Belikov, A., et al. (2016). Theano:

A python framework for fast computation of mathematical expressions. *arXiv preprint arXiv:1605.02688*.

Whittington, J. C. and Bogacz, R. (2017). An approximation of the error back-propagation algorithm in a predictive coding network with local hebbian synaptic plasticity. *Neural Computation*, 29(5):1229–1262.

Whittington, J. C. and Bogacz, R. (2019). Theories of error back-propagation in the brain. *Trends in cognitive sciences*.

Xie, X. and Seung, H. S. (2000). Spike-based learning rules and stabilization of persistent neural activity. In *Advances in neural information processing systems*, pages 199–208.

Xie, X. and Seung, H. S. (2003). Equivalence of backpropagation and contrastive hebbian learning in a layered network. *Neural computation*, 15(2):441–454.

Yamins, D. L. and DiCarlo, J. J. (2016). Using goal-driven deep learning models to understand sensory cortex. *Nature neuroscience*, 19(3):356.